

## Effect of aspect ratio and fluid elasticity on chain orientation in isothermal film casting process

Joo Sung Lee\* and Ju Min Kim\*\*<sup>†</sup>

\*Battery R&D, LG Chem/Research Park, Daejeon 305-380, Korea

\*\*Department of Chemical Engineering, Ajou University, Suwon 443-749, Korea

(Received 10 August 2009 • accepted 2 November 2009)

**Abstract**—The characteristics of extensional flow and the chain orientations of the isothermal film casting process utilizing a two-dimensional (2-D) viscoelastic model with finite element methods (FEM) were studied. Steady state and transient solutions were obtained for a relatively large aspect ratio regime by employing successive iterative schemes. In this work, higher aspect ratios of the equipment caused highly oriented molecular structures because the aspect ratio increases as the flow changes from planar to uniaxial extensional flow. Fluid viscoelasticity always alleviated the neck-in phenomenon and led to the planar extension regime even if dichotomous behavior was observed for draw resonance in extensional thickening and thinning fluids. Consequently, the change in the characteristic of extensional deformation from uniaxial deformation to the planar extension deteriorated the molecular orientation.

Key words: Film Casting, Finite Element Method, Chain Orientation, Fluid Viscoelasticity, Extensional Flow

### INTRODUCTION

The film casting process is one of the most important extensional deformation processes in the fabrication of various films for the cutting-edge IT (information technology) or ET (energy technology) industries [1]. For instance, the polarizer and optical compensation films are key components for liquid crystal display (LCD), and the film casting process is utilized to fabricate those items because it guarantees the higher transparency and optical anisotropy needed for display devices. To produce polarizer with high efficiency, it is important to investigate the chain orientation of polymer molecules, which is induced by film stretching. Furthermore, the technologies used in film casting can also be applied to the porous polyolefin separators used in Li-ion batteries to control the uniform film thickness and pore size distribution. In general, the molten polymer is extruded from a T-die and simultaneously stretched in the machine direction by the motion of the rotating chill roll (Fig. 1). The die opening is typically on the order of few millimeters and the final film thickness is reduced to between 5 and 200  $\mu\text{m}$  during the drawing process. In general, the extensional deformation between the T-die and the chill rolls is mainly governed by planar extension flow, although a portion of uniaxial deformation contributes to neck-in and edge bead formation [2]. The mechanical properties of these films are quite different along the machine and transverse directions, since the molecular structure is highly oriented in the machine direction. Most of the time, the final product is made by using only the center region of the film because of uniformity in film thickness by planar extension, and the edge is trimmed by passing it between

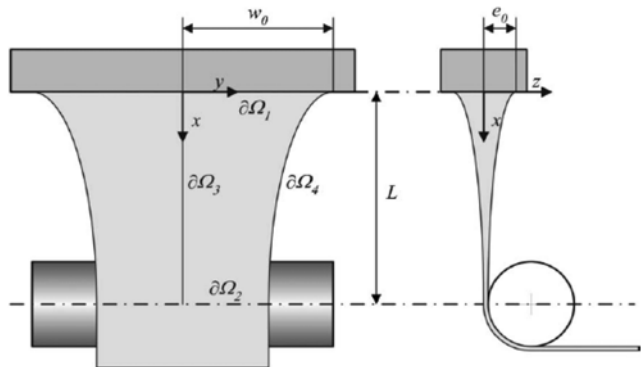


Fig. 1. Schematic diagram of the 2-D isothermal film casting process.

upper and lower rotary blades. Other times a uniaxially deformed film made by controlling process variables (e.g., aspect ratio) is preferred in order to guarantee that the polymer chains are highly oriented.

Many kinds of process disturbances inevitably limit the productivity and uniformity of the film. The defects caused by these disturbances are typically classified into either a transient or steady mode. First, draw resonance, which is characterized by oscillations of all of the state variables such as film thickness, film width, and tension, arises when the drawdown ratio is increased beyond its critical value. The same phenomenon also occurs in other extensional deformation processes, e.g., fiber spinning and film blowing [3,4]. Over the past four decades, draw resonance has attracted a great deal of attention in important stability studies for processes because of its academic and industrial importance as a research topic or a productivity issue [3,4]. Especially, Hyun's group has been devoted to revealing the fundamental mechanism of this interesting instability and investing the draw resonance criterion based on the kinematic wave theory [5-7]. Among the many possible traveling waves in the fiber spinning process, only the unity-throughput waves, which

<sup>†</sup>To whom correspondence should be addressed.

E-mail: jumin@ajou.ac.kr

<sup>‡</sup>This paper is dedicated to Professor Jae Chun Hyun for celebrating his retirement from Department of Chemical and Biological Engineering of Korea University.

start at the spinneret, and the maximum and minimum cross-sectional area waves, which start just after the spinneret, travel the entire spinning distance, whereas the other waves, like constant-area waves, constant-velocity waves, non-unity-throughput waves, travel only a portion of the spinning distance. According to this draw resonance criterion, the critical draw ratio can be determined from the balance between the required traveling time for two successive unity-throughput waves and the allowed traveling time of the maximum and minimum cross-sectional area waves. This criterion can also be predicted using a dominant eigenfunction or the normal mode restricted by the critical draw ratio using linear stability analysis [8]. This draw resonance criterion can be applied not only to the fiber spinning process but also to the other extensional deformation processes such as film casting and blowing. Second, there are the problems with the reduction of the film width along the machine direction, which is called as 'neck-in', and the development of beads at the edge of the film, known as 'edge beads' [2,9]. Even in the steady state, the width of the molten polymer film extruded from a flat die shrinks along the machine direction due to the surface tension at the film's edge.

Since the first work on illuminating the draw resonance instability laid the foundation for studying film casting [10], there have been many research efforts that have studied the dynamics and stability in this process. Co's group interestingly exploited the stability results for viscoelastic fluids [11,12] using a constant 1-D model. Agassant's group developed more refined 1-D models [13], which are capable of explaining neck-in as well as draw resonance, assuming that the deformation rate is constant in both the film width and film thickness directions. Several research groups have made significant strides in the theoretical studies of 2-D film casting. Agassant's group [14] adopted a membrane model consisting of an elastic-like equation for velocity and transport equations for the film thickness and free surfaces. That study was the first to reveal the transient behavior for the Newtonian case using a tracking strategy for a deformed rectangular mesh and a capturing strategy with a continuous finite element for film velocity and discontinuous finite element for film thickness. Recently, the transient responses of viscoelastic 2-D model have been reported to elucidate all of the instabilities observed in the film casting process [15,16].

In this study, the authors have theoretically investigated the effects of both fluid viscoelasticity in polymer melts and the aspect ratio of the equipment on the process stability and chain orientation using both a steady state solution and transient response of a 2-D isothermal film casting model.

## MODELING

Based on the film casting models used in previous studies, the governing equations for the isothermal 2-D system are shown below for Phan-Thien Tanner (PTT) fluids [14-16]. Fig. 1 represents the schematic geometry and boundaries for this system. If the film curvature is small enough, the total stress in normal direction of the film ( $\sigma_z$ ) should be zero, which means that the isotropic pressure is equal to the normal stress ( $\tau_z$ ).

$$\text{Equation of continuity: } \frac{\partial e}{\partial t} + \nabla \cdot e \mathbf{v} = 0 \quad (1)$$

$$\text{Equation of motion: } \nabla \cdot e \sigma = 0 \quad (2)$$

Constitutive equations (PTT fluids):

$$K \tau + \lambda \left[ \frac{\partial \tau}{\partial t} + \mathbf{v} \cdot \nabla \tau - \mathbf{L} \cdot \tau - \tau \cdot \mathbf{L}^T \right] = 2 \eta \mathbf{D} \quad (3)$$

$$\text{where, } K = \exp \left( \frac{\varepsilon}{G} \text{tr } \tau \right), \quad \mathbf{L} = \nabla \mathbf{v} - \xi \mathbf{D}$$

Boundary conditions

$$\text{i) Inlet: } v_x = v_0, v_y = 0, e = e_0 \text{ on } \partial \Omega_1 \text{ at } t = 0 \quad (4a)$$

$$v_x = v_0, v_y = 0, e = e_0, \tau = \tau_0 \text{ on } \partial \Omega_1 \text{ at } t > 0$$

$$\text{ii) Outlet: } v_x = v_L, v_y = 0 \text{ on } \partial \Omega_2 \text{ at } t = 0 \quad (4b)$$

$$v_x = v_L(1 + \delta), v_y = 0 \text{ on } \partial \Omega_2 \text{ at } t > 0$$

$$\text{iii) Center: } \sigma_{xy} = 0 \text{ on } \partial \Omega_3 \text{ at } t \geq 0 \quad (4c)$$

$$\text{iv) Edge: } \frac{\partial w}{\partial t} + v_x \frac{\partial w}{\partial y} = v_y, \quad \sigma \cdot \mathbf{n} = 0 \text{ on } \partial \Omega_4 \text{ at } t \geq 0 \quad (4d)$$

The important dimensionless groups of this system are the Deborah number (De), representing the extent of fluid viscoelasticity, and the aspect ratio ( $A_r$ ), which is defined by the ratio between half of the width of the T-die and the drawing distance. The film casting flow was analyzed using the governing equations with the finite element method (FEM), which was developed by Kim et al. [15] and Shin et al. [16]. Since the convection terms in the continuity and kinematic equations could destabilize the overall system numerically, the streamline upwinding/Petrov Galerkin (SU/PG) method was employed [17,18]. Moreover, uniformly distributed rectangular meshes were used at the initial stage, and the locations of the inner nodes were redistributed using the spine method. Despite these numerical schemes, it was difficult to directly obtain solutions that converged at high aspect ratios (i.e.,  $A_r > 1.0$ ). In those cases, the aspect ratio was successively incremented from a low value to the target value, where the solution for the lower aspect ratio was used as initial guess. Solutions were obtained at high  $A_r$  values using this strategy. The optimal mesh tessellation used here was a  $25 \times 25$  rectangular mesh, which guaranteed an acceptable accuracy and high efficiency [15]. It was important to set the stress boundary conditions at the die-exit, because an inappropriate selection would negatively effect the numerical convergence [19,20], even though the boundary conditions for the stress tensor did not have a great influence on the final solutions. For the transient simulation, a step disturbance was introduced into the system on the outlet velocity boundary condition in order to examine the propagation of the initial disturbance and to determine process stability.

## RESULTS AND DISCUSSION

Generally, the film casting process is operated in the low aspect ratio regime (i.e.,  $A_r < 1.0$ ) to prevent the neck-in phenomenon [1]. The velocity in the transverse direction was relatively low during stretching as shown in Fig. 2(a). By employing successive iterative schemes, the aspect ratio range was expanded up to 5 to explore the characteristics of the extensional deformation in the film casting process. It is not only meaningful to analyze the process but also to estimate its properties. To make highly oriented film such as a polarizer, the aspect ratio of the stretching device equipment is generally high (i.e.,  $A_r > 3.0$ ). In the case of a high aspect ratio ( $A_r = 3.5$ ), the neck-in phenomenon conspicuously occurred, and the final

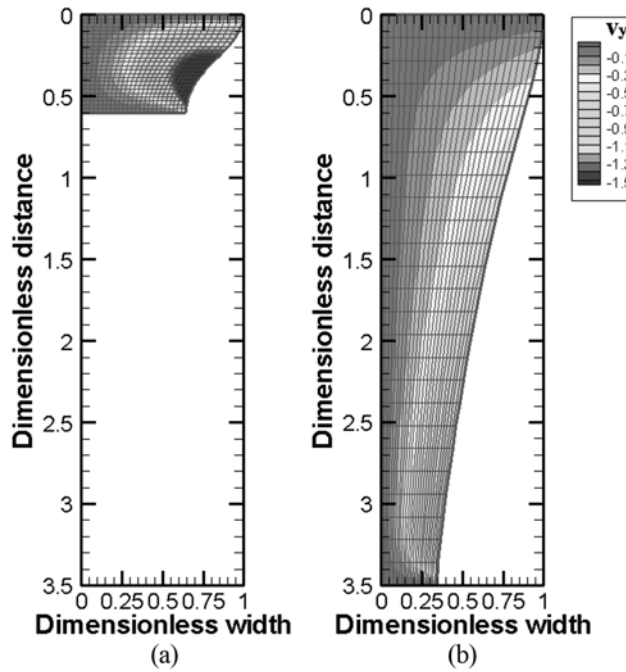


Fig. 2. Velocity contour in the transverse direction for both the (a) low aspect ratio ( $A_r=0.6$ ) and (b) high aspect ratio ( $A_r=3.5$ ) condition at  $D_r=10$  and  $De=0.001$ .

film width remained less than half of the initial film width as shown in Fig. 2(b). Based on the conceptual approach of the Dobroth-Erwin model [2], the central part of a molten film maintained the planar deformation while the edge part underwent uniaxial deformation due to the neck-in phenomena. Similar to a typical film casting process, the extensional deformation no longer had planar extension at the high aspect ratio condition because of the large reduction in the film width. Therefore, the majority of the stretched film region shifted to uniaxial extension. To systematically explain the extension characteristic, the extensional flow characteristic parameter ( $\gamma$ ) was introduced in Eq. (5). This parameter can be derived from the strain ( $d$ ) in each direction. During film stretching, the extensional flow characteristic parameter varies from zero (uniaxial extension) to one (planar extension).

$$\gamma = \frac{d_y \sqrt{d_x} - 1}{\sqrt{d_x} - 1} \quad (5)$$

where,  $d_x$  is the velocity ratio between the die exit and chill roll ( $=v_L/v_0$ ) which is calculated using thickness reduction and width reduction (i.e.,  $v_L/v_0 = e_L w_0/e_L w_L$ ), and  $d_y$  is the width ratio between die exit and chill roll ( $=w_L/w_0$ ).

As shown in Fig. 3, the extensional flow characteristic parameter had a lower value at the edge, which corresponds to uniaxial-like extensional flow, whereas a higher  $\gamma$  value was observed at the center of drawn film caused by edge beads. The film width rapidly decreased compared to film thickness as the aspect ratio increased. The thickness was not greatly affected because the thickness reduction was set by the draw ratio, not the aspect ratio. For this reason, the extensional deformation in the higher aspect ratio regime is close to uniaxial extension.

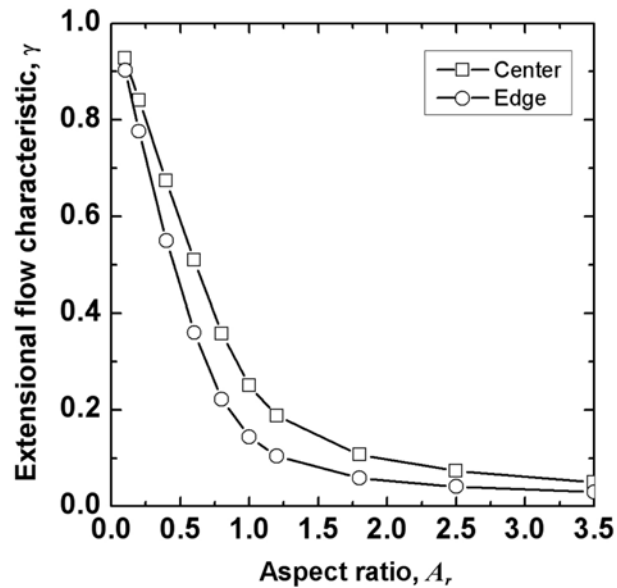


Fig. 3. Effect of the aspect ratio on the degree of planar extension at the center of film and the edge under the same operating conditions as Fig. 2.

Generally, uniaxial extension flow is more advantageous than planar extensional flow with respect to the polymer chain orientation. To illustrate this point, Herman's orientation function ( $f$ ) was introduced which using Eq. (6) [21]. Herman's orientation function, which relates optical birefringence to the segmental orientation, is probably the most frequently used quantity characterizing the orientation. Herman's orientation function takes value 1 for a system with complete orientation to stretching direction and 0 for non-orientated film. Herman's orientation function can be rewritten using the strain in the stretching direction ( $d_x$ ) and the extensional flow characteristic parameter ( $\gamma$ ) represented in Eq. (5).

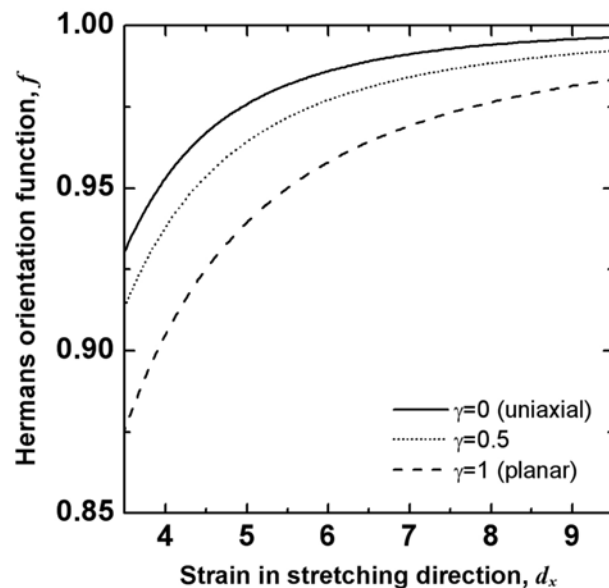
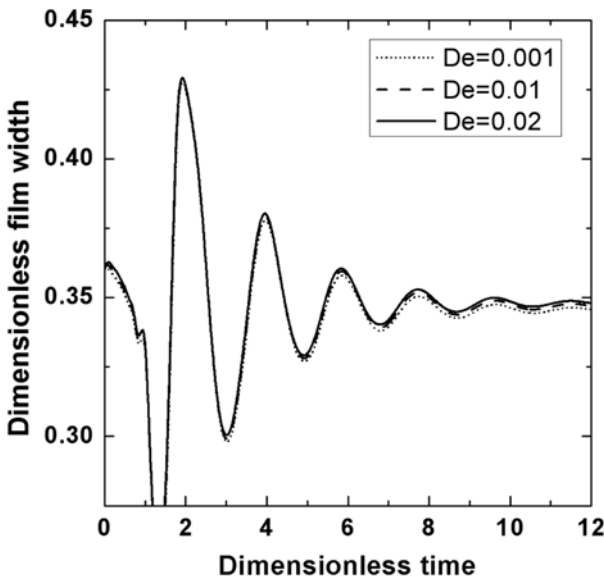


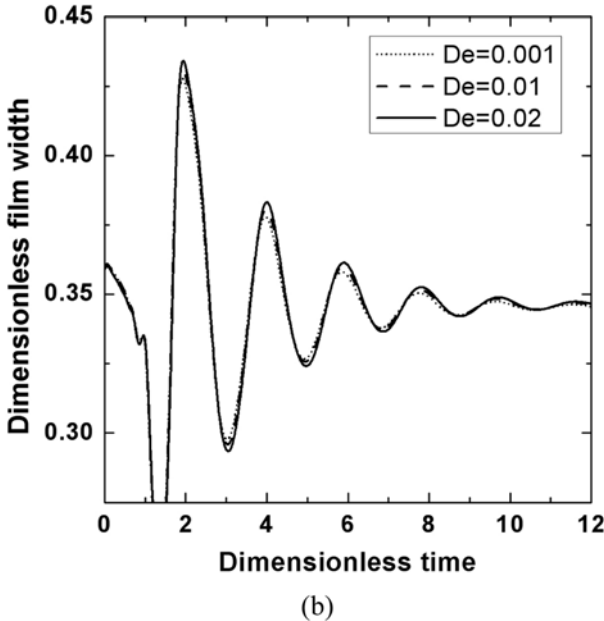
Fig. 4. Effect of the characteristic of extensional deformation on the orientability.

$$\begin{aligned}
 f &= \frac{3\langle \cos^2 \psi \rangle - 1}{2} = \frac{1}{2} \left( \frac{3d_x^2}{d_x^2 + d_y^2 + d_z^2} - 1 \right) \\
 &= \frac{1}{2} \left( \frac{3d_x^2}{d_x^2 + \frac{[(\sqrt{d_x} - 1)\gamma + 1]^2}{d_x} + \frac{1}{[(\sqrt{d_x} - 1)\gamma + 1]^2 d_x}} - 1 \right) \quad (6)
 \end{aligned}$$

where  $\psi$  denotes the angle between flow direction and chain segment and  $\langle \rangle$  means the averaged value. As shown in Fig. 4, Hermann's orientation function was naturally related to the strain in stretching direction and showed a higher dependency on the extensional flow characteristic. The molecules for uniaxial flow ( $\gamma=0$ ), were



(a)

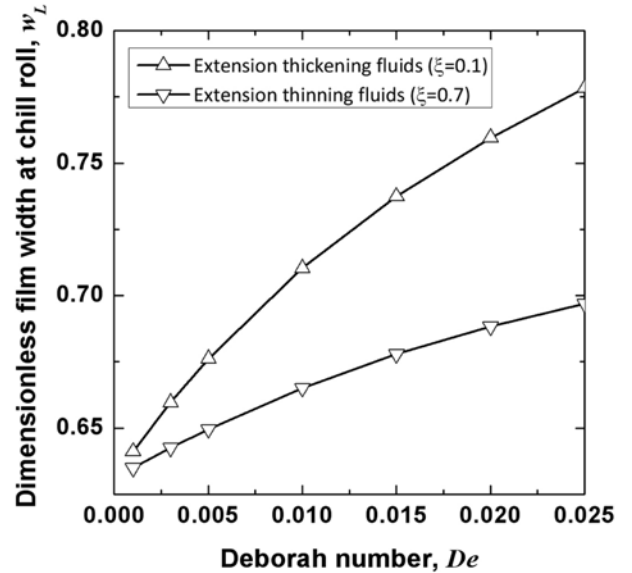


(b)

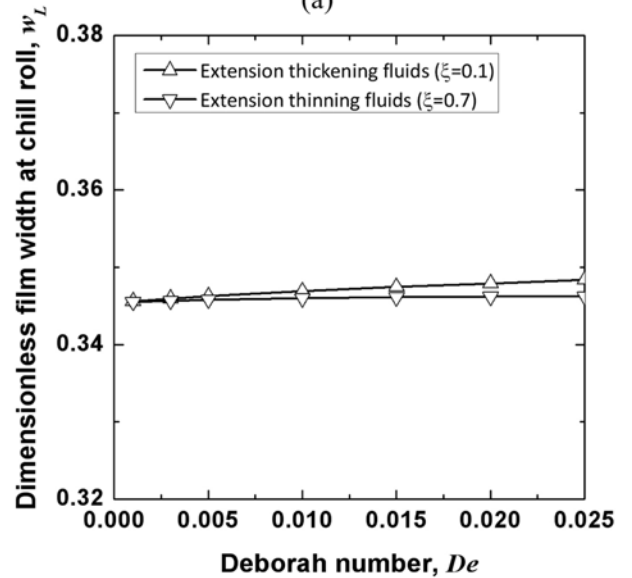
Fig. 5. Transient responses of the dimensionless film width for (a) extensional thickening fluids and (b) extensional thinning fluids at  $D_r=10$  and  $A_r=3.5$ .

more highly oriented in the flow direction at the same strain than the molecules of planar ( $\gamma=1$ ) or mixed extensional flow ( $0 < \gamma < 1$ ). Therefore, a high aspect ratio was favorable for making highly oriented films because uniaxial extensional flow is dominant at higher aspect ratios.

Fluid viscoelasticity has a dichotomous behavior between extensional thickening and thinning fluids in extensional deformation processes such as fiber spinning, film casting and blowing. This has been systematically analyzed by Hyun's group using linear and nonlinear stability analyses [3,16,22]. Fluid viscoelasticity clearly contributed to the reduction of process (or tension) sensitivity for extensional thickening fluids such as low-density polyethylene (LDPE), whereas fluid viscoelasticity led to an increase in the process sensi-



(a)



(b)

Fig. 6. The change in dimensionless width at the chill roll ( $w_L$ ) caused by changing the fluid viscoelasticity for extensional thickening and thinning fluids at  $D_r=10$  under the (a) low aspect ratio ( $A_r=0.6$ ) and (b) high aspect ratio ( $A_r=3.5$ ).

tivity for extensional thinning fluids such as high-density polyethylene (HDPE) in the low aspect ratio regime. In previous literature [16,22], a constitutive equation and two parameter sets were chosen to describe extensional thickening and thinning fluids, i.e., the PITT constitutive model was adopted to portray an extensional thickening fluid ( $\varepsilon=0.015$ ,  $\xi=0.1$ ) and an extensional thinning one ( $\varepsilon=0.015$ ,  $\xi=0.7$ ). First, the propagation of the initial step disturbance ( $\delta=10\%$ ) was recorded with time for the high aspect ratio condition ( $A_r=3.5$ ). As seen in Fig. 5, all of the transient solutions showed stable conditions at the given draw ratio, but the fluid viscoelasticity helped to quickly smooth out the initially introduced disturbance for extensional thickening fluids but not for the extensional thinning fluids. However, we note that the effect of fluid viscoelasticity on the process stability diminished as the aspect ratio increased.

The effects of the fluid viscoelasticity on the neck-in for the stable regime are plotted in Fig. 6. While a dichotomous behavior was

found for the draw resonance instability, increasing the fluid viscoelasticity alleviated the neck-in phenomenon for both extensional thickening and thinning fluids. For the low aspect ratio case ( $A_r=0.6$ ) depicted in Fig. 6(a), the Deborah number was critical to the final film width especially for extensional thickening fluids. However, the effect of the fluid viscoelasticity diminished for the high aspect ratio condition ( $A_r=3.5$ ) as plotted in Fig. 6(b), even though their trends were qualitatively similar for the neck-in phenomenon. These differences in the final film width affected the extensional flow characteristic parameter and the chain orientation. Moreover, the formation of edge beads induced a difference in the deformation characteristic between film's center and edge. As shown in Fig. 7(a), the characteristic of extensional deformation changed to planar extension due to the fluid viscoelasticity and had higher value (i.e., it moved to the planar extension regime) at the center of the film for the low aspect ratio condition ( $A_r=0.6$ ). On the other hand, the ex-

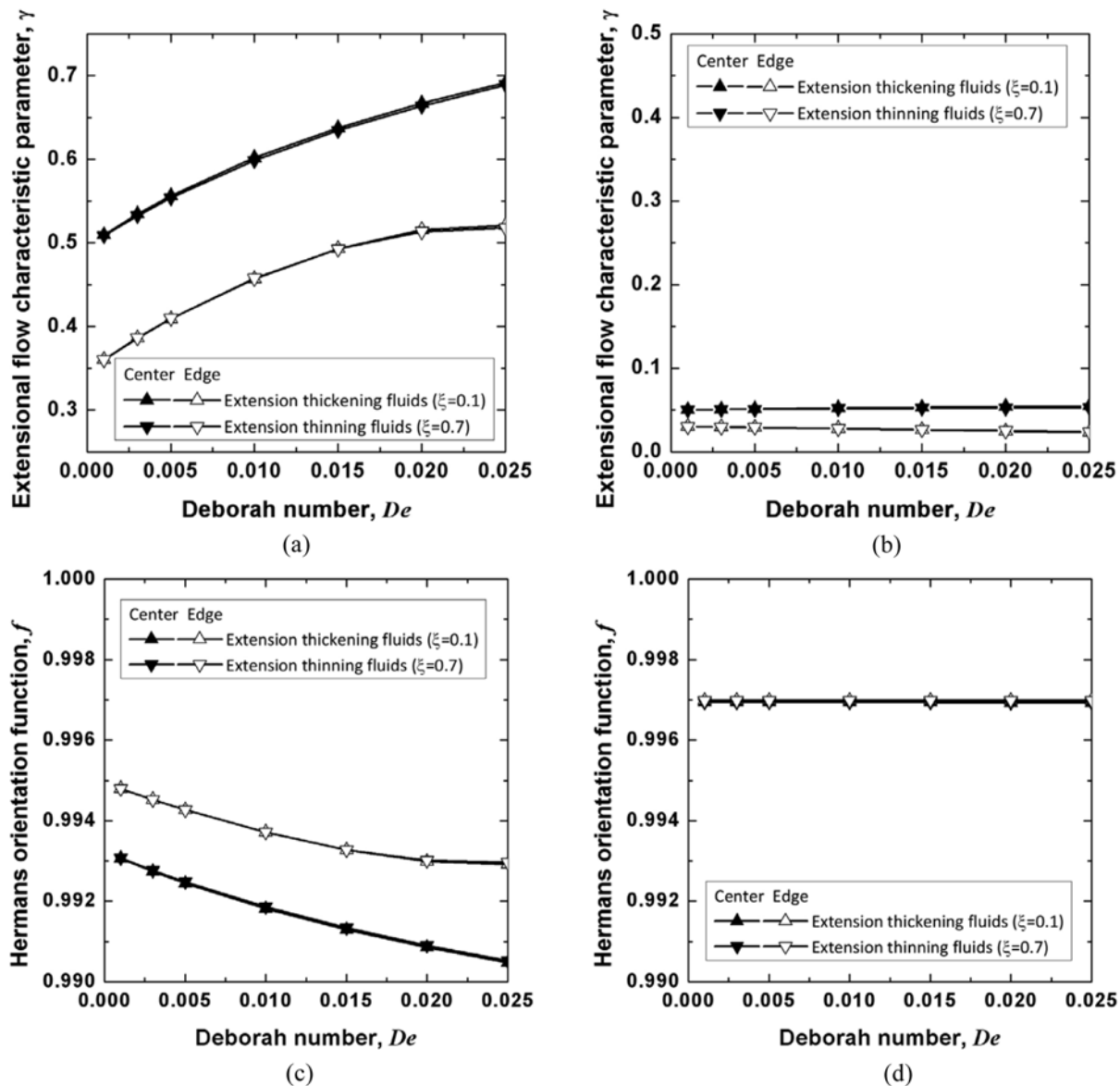


Fig. 7. The change in the degree of planar extension ( $\gamma$ ) and molecular orientation ( $f$ ) at the film's center and edge positions caused by changing fluid's viscoelasticity.

tensional flow characteristic parameter showed almost uniaxial extension flow for the high aspect ratio condition ( $A_r=3.5$ ) as seen in Fig. 7(b). The difference between film center and edge for the high aspect ratio was greater than low aspect ratio. As the aspect ratio increased, the flow characteristic led to the uniaxial deformation due to highly neck-in, and the flatness of the final film thickness (i.e., less edge beads) led to uniformity of the extension characteristic in the transverse direction. Moreover, these changes were insensitive to the fluid viscoelasticity in the case of the high aspect ratio, which was similar to the reduction of film width plotted in Fig. 6. As mentioned before, the polymer chains were highly oriented under uniaxial extensional flow so that the edge position showed a higher orientation than the center of the film at the same draw ratio as shown in Fig. 7(c). The higher fluid viscoelasticity helped to stabilize the film casting process for extensional thickening fluids, but it deteriorated the chain orientation for both extensional thickening and thinning fluids. However, these effects became insignificant when the extensional deformation showed uniaxial extension characteristics. Especially for the high aspect ratio condition, the edge beads disappeared during stretching, and the film thickness was uniform in transverse direction. As shown in Fig. 7(d), the film casting process became very robust to manipulating variables, and uniform orientation can be achieved in the transverse direction of the stretched film.

## CONCLUSIONS

The characteristics of extensional flow and the chain orientations in a 2-D isothermal viscoelastic model of the film casting process have been investigated using finite element methods (FEM). By adopting successive iterative schemes, the convergence range of aspect ratio was increased to 5 so that the deformation characteristic and chain orientation could be described in the high aspect ratio regime. Even though fluid viscoelasticity for extensional thickening and extensional thinning fluids showed a dichotomous behavior for the process stability (or draw resonance), the neck-in phenomenon was always alleviated as the De number increased and led to planar extension for both extensional thickening and extensional thinning fluids. This was consequently harmful to making a highly oriented film. Higher aspect ratios of the equipment led to highly oriented molecular structures because of the uniaxial extension characteristic caused by the neck-in phenomenon, and the structures showed robustness to variation of other manipulating variables. This information about the flow characteristic and orientation will be useful in designing the stretching process for optical films (e.g., polarizer, and optical compensation films), and will guarantee high polarizing efficiency for liquid crystal display (LCD) industry.

## ACKNOWLEDGMENT

This research was supported by Basic Research Program through the National Research Foundation of Korea (NRF) funded by the Ministry of Education, Science and Technology (No. 2009-0074230).

## NOMENCLATURE

$A_r$  : aspect ratio [ $\equiv L/w_0$ ]  
 $\mathbf{d}$  : strain tensor

<b>D</b>	: rate of deformation tensor
De	: deborah number [ $\equiv \lambda v_0/L$ ]
$D_r$	: draw ratio [ $\equiv v_L/v_0$ ]
e	: film thickness
L	: distance from die to chill roll
$\mathbf{n}$	: normal vector
t	: elapsed time
$\mathbf{u}$	: velocity vector with component u and v for x- and y-direction, respectively
w	: film width
$\varepsilon, \zeta$	: PTT model parameters
$\psi$	: angle between flow direction and chain segment
$\gamma$	: parameter for extensional flow characteristic
$\eta$	: zero shear viscosity
$\sigma$	: total stress tensor
$\tau$	: stress tensor

## Subscript

0	: die exit
L	: chill roll position
x	: flow direction (machine direction)
y	: transverse direction
z	: normal direction to the film surface

## REFERENCES

1. T. Kanai and G. A. Campbell, *Film processing*, Hanser Publishers, Cincinnati (1999).
2. T. Dobroth and L. Erwin, *Polym. Eng. Sci.*, **26**, 462 (1986).
3. H. W. Jung and J. C. Hyun, *Fiber spinning and film blowing instabilities in polymer processing instabilities: Control and understanding*, S. G. Hatzikiriakos and K. B. Migler Eds., Marcel Dekker, New York (2005).
4. A. Co, *Draw resonance in film casting in polymer processing instabilities: Control and understanding*, S. G. Hatzikiriakos and K. B. Migler Eds., Marcel Dekker, New York (2005).
5. J. C. Hyun, *AIChE J.*, **24**, 418 (1978).
6. B. M. Kim, J. C. Hyun, J. S. Oh and S. J. Lee, *AIChE J.*, **42**, 3164 (1996).
7. H. W. Jung, H.-S. Song and J. C. Hyun, *AIChE J.*, **46**, 2106 (2000).
8. J. S. Lee, H. W. Jung, J. C. Hyun and L. E. Scriven, *AIChE J.*, **51**, 2869 (2005).
9. H. Ito, M. Doi, T. Isaki and M. Takeo, *J. Soc. Rheol. Jpn.*, **31**, 157 (2003).
10. Y. L. Yeow, *J. Fluids Mech.*, **66**, 613 (1974).
11. N. R. Anturkar and A. Co, *J. Non-Newtonian Fluid Mech.*, **28**, 287 (1998).
12. V. R. Iyengar and A. Co, *Chem. Eng. Sci.*, **51**, 1417 (1996).
13. D. Silagy, Y. Demay and J. F. Agassant, *Polym. Eng. Sci.*, **36**, 2614 (1996).
14. D. Silagy, Y. Demay and J. F. Agassant, *J. Non-Newtonian Fluid Mech.*, **79**, 563 (1998).
15. J. M. Kim, J. S. Lee, D. M. Shin, H. W. Jung and J. C. Hyun, *J. Non-Newtonian Fluid Mech.*, **132**, 53 (2005).
16. D. M. Shin, J. S. Lee, J. M. Kim, H. W. Jung and J. C. Hyun, *J. Rheol.*, **51**, 393 (2007).
17. A. N. Brooks, T. J. R. Hughes, *Comput. Methods Appl. Mech. Eng.*,

32, 199 (1982).

18. K. B. Sunwoo, S. J. Park, S. J. Lee, K. H. Ahn and S. J. Lee, *J. Non-Newtonian Fluid Mech.*, **99**, 125 (2001).

19. D. Rajagopalan, *J. Rheol.*, **43**, 73 (1999).

20. C. Sollogoub, Y. Demay and J. F. Agassant, *J. Non-Newtonian Fluid Mech.*, **138**, 76 (2006).

21. U. W. Gedde, *Polymer Physics*, Kluwer (1995).

22. S. W. Choi, D. M. Shin, J. S. Lee, J. M. Kim, H. W. Jung and J. C. Hyun, *Korean J. Chem. Eng.*, **26**, 26 (2009).